Multi-Physical Model of Li-Ion Battery Based on Aging Experimental Results

Solomon Berihu Araya, Dr. Daniela CHRENKO, Dr. Alexandre RAVEY, Prof. Fei GAO
Université Marie et Louis Pasteur, UTBM, CNRS, institute FEMTO-ST, F-90000 Belfort, France
solomon.araya@utbm.fr

RESUME

This paper presents a multi-physical model of a lithium-ion battery based on laboratory experimental data to simulate battery behavior and aging, which integrates an Equivalent Circuit Model (ECM), a two-dimensional (2D) thermal model, and an empirical aging model. The ECM simulates the electrical response of a commercial 40 Ah NMC pouch cell and is parametrized using Electrochemical impedance spectroscopy (EIS) data. The 2D thermal model based on the heat diffusion equation computes the spatial temperature distribution within the cell using the heat generation. The aging model employs Arrhenius-type stress factor formulation to predict the capacity fade. All sub-models are coupled in a way that the ECM model feeds heat generation to the thermal model, which provides the cell temperature to the aging model, and the aging model updates the ECM parameters. Validation using experimental data proves the model accurately captures the cell impedance spectrum across different states of charge and different temperature values, the surface temperature at multiple locations, and the capacity fade across several cycles. This model provides the estimation of key battery state indicators like the SOC, temperature distribution, and state of health (SOH).

Keywords— lithium-ion battery aging, battery management system, remaining useful life, multi-physical modeling, digital twin

1. INTRODUCTION

Batteries are essential to advancing renewable energy use in transportation, with lithium-ion (Li-ion) batteries dominating due to their high energy density, cycle life, and suitability for mobile applications [1]. However, the performance and lifetime of Li-ion batteries are limited by complex aging phenomena, making effective Battery Management Systems (BMS) necessary to ensure safety and optimized performance. Thus, accurate models are essential for BMS to predict state of charge (SOC), state of health (SOH), and the remaining useful life (RUL), as poor battery life estimations can lead to early end-of-life and significant economic losses.

Multiphysics models that incorporate Electrical behaviour, heat generation, and degradation have shown promising results. To address these aspects, various researchers have proposed integrated modelling approaches that aim to represent the coupled electrical, thermal, and aging behaviour of batteries. [2] and [3] developed a semi-empirical aging model that couples a Thevenin equivalent circuit with a lumped thermal network to predict cycle and calendar aging with low computational cost. Likewise, [4] proposed a Thevenin ECM model and lumped thermal model to capture both cycle and calendar aging effects on capacity and resistance. A lumped multi-physics model with an adaptive parameter identification for online SOH estimations has also been developed in [5]. However, those studies didn't consider the spatial temperature distribution and are focused on cylindrical cells.

The Horizon Europe ENERGETIC project aims to address these challenges by developing new sensing technologies and combining Multiphysical and AI-driven modeling to predict battery behavior accurately with a digital twin. This project contributes to the digital twin framework by applying a continuous 2D model to a large pouch cell and explicitly coupling it to the ECM and an empirical aging model. This model gives more detailed information to the BMS about the battery behavior and can track how hot spots develop with cell aging, enabling SOH prediction. All the model parameters are calibrated using laboratory experimental data, using EIS test results to fit the ECM model, separate thermal test results to validate the 2D thermal model, and cycling tests to calibrate the capacity fade model. The rest of the article is organized as follows: Section 2 outlines the modelling approach, Section 3 describes the methodology and experimental setup, Section 4 discusses the results, and the article closes with conclusions and future perspectives in Section 5.

2. MODELING APPROACH

2.1 Equivalent Circuit Model (ECM)

The equivalent circuit model (ECM) is one of the most widely used approaches to simulating a battery's electrical and thermal behaviors. This method simplifies the battery's internal complex electrochemical processes into manageable electrical components that involve resistors, capacitors, and voltage sources [6], [7].

Various studies have proposed different ECM models, starting from a simple one with resistance in series with open circuit voltage (OCV), to more complex models with many RC branches to simulate the battery behavior [7]. In this paper, the ECM is developed based on the EIS result of the pouch cell and is described in Figure 1, where the CPE represents a constant phase element.

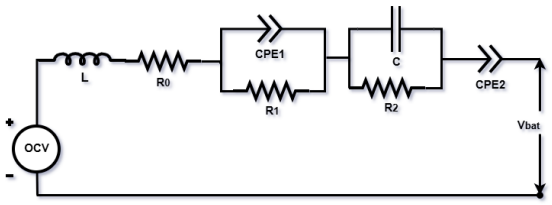

Figure 1: Proposed ECM model

Once the ECM is developed, the next step is the extract the ECM parameters, and it is done by fitting the model to the EIS test results. In [6], many approaches are discussed for extracting ECM parameters. In this paper, the model parameters are extracted based on a non-linear least square method and Eq. (1) describes total impedance of the proposed ECM model.

$$Z_{Model} = j\omega L + R_0 + \frac{R_1}{1+R_1*Q_1(j\omega)^{n_1}} + \frac{R_1}{1+R_1*Q_1(j\omega)^{n_1}} + \frac{R_2}{1+j\omega R_2*C} \quad (1)$$

Thus, the estimation of the total impedance has 9 parameters listed in Eq. (2).

$$Z_{Model} = f(L,\ R_0, R_1, Q_1, n_1, R_2, C, Q_2, n_2) \quad (2)$$

A. Heat generation

In this paper, the ECM parameters are used to determine the heat generated inside the cell. The heat generated during the battery operation contains the reversible and irreversible heat [8].

The irreversible heat generation is derived from the electrical losses calculated in the ECM and is described by Eq. (3).

$$Q_{irr} = I^2R \quad (3)$$

where, R is the internal resistance in ohms.

The reversible heat due to the entropy change is also described in Eq. (4).

$$Q_{rev} = -I\left(T\frac{dV_{ocv}}{dT}\right) \quad (4)$$

The entropic coefficient here is determined by using a potentiometric method that involved measuring the open circuit potential (OCP) of a cell at different temperatures.

The total heat generated by the battery is then calculated using Eq. (5):

$$q = I^2R - I\left(T\frac{dV_{ocv}}{dT}\right) \quad (5)$$

2.2 Thermal Model

Another key aspect of lithium-ion battery modeling is thermal modeling, which is crucial in understanding the thermal behaviour and essential for cooling during battery operation, with studies showing that efficient cooling systems can enhance battery lifespan [9]. Papers in [10] [11] present a lumped thermal and heat generation model for Li-ion batteries, which helps characterize and simulate the thermal behaviour under different conditions, but they didn't consider spatial temperature distribution.

The model in this work is based on the 2D heat diffusion equation with internal heat generation, and the heat conduction equation is discretized using the Finite Difference Method (FDM) on a 2D grid. The thermal model captures the temperature distribution within the Li-ion battery pouch cell during operation with the thermocouple positions as shown in Figure 2.

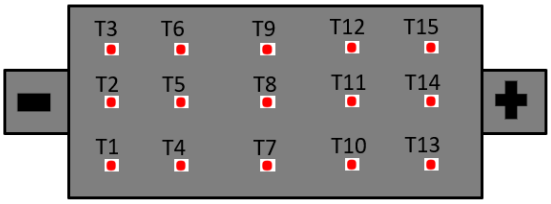

Figure 2: Thermocouples position on the pouch cell

The temperature distribution in the two dimensions x and y of the cell is given in Eq. (6):

$$\rho c_p = \left(\frac{dT}{dt}\right) = k_x\left(\frac{\partial^2 T}{\partial x^2}\right) + k_y\left(\frac{\partial^2 T}{\partial y^2}\right) + q \quad (6)$$

where, ρ is density of the cell in kg/m^3, c_p is specific heat capacity in J/kg.K, h is heat transfer coefficient in W/m2.K, $k_x$and k_y are the thermal conductivity in of the cell in the x and y direction in W/m.K.

The FDM of the heat conduction equation is:

$$\begin{cases} \dfrac{dT}{dt} = \dfrac{T_{i,j}^{n+1} - T_{i,j}^{n}}{\Delta t} \\ \dfrac{\partial^2 T}{\partial x^2} = \dfrac{T_{i,j+1}^{n} - 2T_{i,j}^{n} + T_{i,j-1}^{n}}{\Delta x^2} \\ \dfrac{\partial^2 T}{\partial y^2} = \dfrac{T_{i,j+1}^{n} - 2T_{i,j}^{n} + T_{i,j-1}^{n}}{\Delta y^2} \end{cases}$$

The following boundary condition is applied at the surface of the pouch cell, considering convective cooling (air cooling).

$$\rho c_p \frac{\partial T}{\partial t} = h(T_{amb} - T) \quad (7)$$

Thus, the temperature values for the internal nodes i,j which depend on the conduction is described by Eq. (8).

$$\left\{T_{i,j}^{n+1} = T_{i,j}^{n} + \Delta t\left[\left(\frac{k_x}{\rho c_p}\frac{T_{i,j+1}^{n} - 2T_{i,j}^{n} + T_{i,j-1}^{n}}{\Delta x^2}\right) + \left(\frac{k_y}{\rho c_p}\frac{T_{i,j+1}^{n} - 2T_{i,j}^{n} + T_{i,j-1}^{n}}{\Delta y^2}\right) + \frac{q}{\rho c_p}\right]\right. \quad (8)$$

where, $T_{i,j}$ is the temperature value of the node i,j.

The temperature for the non-internal nodes i,j, which accounts for the convection (air) cooling, is also given by Eq. (9)

$$\begin{cases} T_{i,j}^{n+1} = \\ T_{i,j}^{n} + \Delta t \left[\frac{k_x}{\rho c_p} \frac{T_{i,j+1}^{n} - 2T_{i,j}^{n} + T_{i,j-1}^{n}}{\Delta x^2} + \frac{k_y}{\rho c_p} \frac{T_{i,j+1}^{n} - 2T_{i,j}^{n} + T_{i,j-1}^{n}}{\Delta y^2} + \right. \\ \left. \frac{q}{\rho c_p} + \frac{h}{\rho c_p} \left(T_{amb} - T_{i,j}^{n} \right) \right] \end{cases} \quad (9)$$

where, $\alpha = \Delta t \frac{k_x}{\rho c_p \Delta x^2}$

The temperature equations, Eq. (8) and Eq. (9), can be formulated in a matrix form using Eq. (10).

$$AT^{n+1} = BT^{n} + Q \quad (10)$$

2.3 Aging model

The aging model tracks the battery SOH over time by defining the ratio of the current capacity to the new capacity, usually expressed as a percentage. It is measured using capacity fade, which indicates the loss of lithium inventory or active material, and resistance growth, which indicates the increase in internal and polarization resistance [12] .

The aging model is influenced by the stress factors, which are the temperature, cycle count, depth of discharge (DOD), and C-rate [13].

The model which formulated based on those stress factors and the Arrhenius-type formulation is stated in Eq. (11) and Eq. (12).

Capacity loss (Q_{loss}):

$$Q_{loss} = B(C_{rate}) \exp\left(\frac{-E_a(C_{rate})}{R.T_{Max}}\right) (A_{th}(N))^{z} \quad (11)$$

where, the Cumulative charge throughput (Ah) is :

$$A_{th}(N) = DOD * N * Nominal\ capacity$$

Resistance growth (ΔR):

$$\Delta R = B(a_0 + a_1 N + a_2 N^2 + \cdots) \exp\left(\frac{-E_a}{R.T_{Max}}\right) \quad (12)$$

where, $B(C_{rate})$ is the Empirical pre-exponential factor, E_a is Activation energy, R is Universal gas constant (8.314 J/mol·K), T_{Max} is the maximum surface temperature in °C, $A_{th}(N)$ is the cumulative charge throughput in Ah, z is Exponential constant, N is the Number of charge-discharge cycles, ΔR is an Increase in internal resistance, B is the pre-exponential factor, and a_0, a_1, a_2 Empirical coefficients are determined from fitting experimental data.

In this work, a cycle aging is carried out at a C-rate of 1C for full charging and discharging at 25°C. Thus, the following aging parameters in Table 1 are determined by fitting with the experimental result using the non-linear least squares method.

Table 1: Aging parameters

B	E_a(J/mol)	Z	RMSE
5.7515e-01	24027.39	1.32915	0.7532

In this case, the temperature is taken from the 2D thermal model by taking the maximum temperature from the 15 sensors to represent the worst-case scenario.

2.4 Coupled multiphysical model

The coupled Multiphysical model integrates ECM with thermal and aging components to capture temperature effects on battery performance and lifespan, which is crucial for mobile applications.

The model characterizes the battery's electrical behaviour and calculates the heat generation using the internal resistances from the ECM. The heat generated from the ECM is an input to the 2D thermal model that computes the temperature distribution across the surface of the pouch cell. The temperature from the thermal model is fed to the aging model, which predicts the capacity loss and resistance growth based on the aging stress factors. Then, the updated resistance growth is fed back to the ECM to update the ECM parameters based on its SOH. Figure 3 illustrates the coupled multiphysical model used in this work.

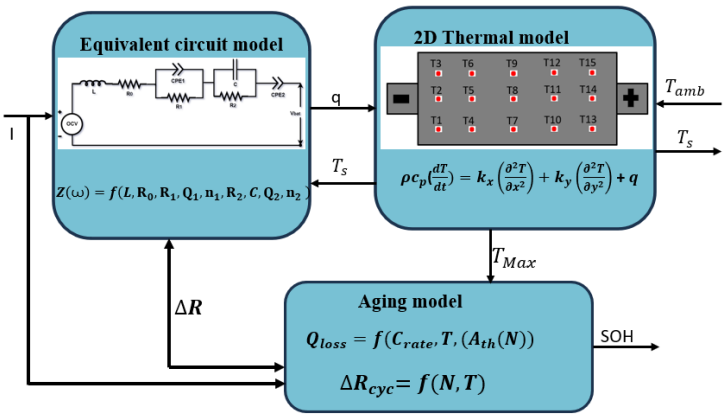

Figure 3: Coupled Multiphysical Model

3 Methodology and Experimental Setup

3.1. Battery cell specifications

The cell used in this research work is a commercial Li-ion 40 Ah pouch cell, and the battery cell specifications are indicated in Table 1.

Table 1: Battery cell specifications

Specification	Value
Cell Model	SPIM11309102-GL40
Cathode	NMC
Anode	Graphite

Nominal Capacity	40 Ah
Nominal Voltage	3.65 V
Cut-off Voltages	2.5 – 4.2 V
Weight	730 ± 15 g
Dimensions (L × W × T)	309 × 102 × 11.2 mm
Thermal Conductivity	1.25 $W \cdot m^{-1} \cdot K^{-1}$
Specific heat Capacity	0.47 $J \cdot g^{-1} \cdot K^{-1}$

3.2. Battery Cell Characterization

A. Electrochemical Impedance Spectroscopy (EIS)

Electrochemical Impedance Spectroscopy (EIS) is a non-destructive technique that provides insights into the internal resistance and overall health of the battery by applying a small AC signal and measuring the impedance.

EIS tests using the Zahner EIS system have been used to characterize the battery behavior and to extract the parameters of ECM. An AC excitation of 2A is used to carry out the EIS test at a frequency range of 50mHz to 1kHz.

B. Aging Tests

The cycling test is one of the most common test techniques used in current standards. This test involves repeatedly charging and discharging the battery to simulate aging over time. It simulates the typical usage pattern of the battery in its intended application. The cycling is performed at a C-rate of 1C for charging and discharging.

Figure 4 illustrates the testing facility at the FEMTO-ST lab, which is used for both EIS and aging experiments. The setup includes the Chroma 17010 Cell tester (A), capable of handling up to 60A and a voltage of 6V for a single channel. Battery cells (C) are placed inside the chamber (B) for thermal stability during the test. Test procedures and data acquisition are managed by the battery lab expert software (D), which allows real-time monitoring and precision control. For EIS characterization, the Zahner EIS instrument (F) is available with its dedicated EIS software (E) to capture the impedance spectra.

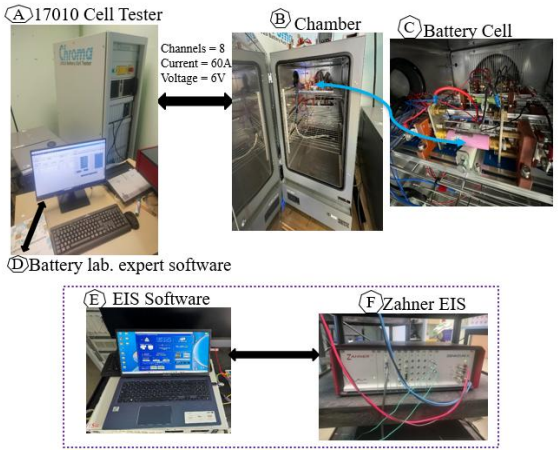

Figure 4: FEMTO-ST testing facility

4 Results and Discussion

The results demonstrate that the ECM model accurately represents the electrochemical behavior of the battery. Figure 5 shows the Nyquist plot of experimental EIS data and the model results at 40°C and different SOC levels, and Figure 6 illustrates the comparison between the model and the experimental data at 90% SOC and different temperature values.

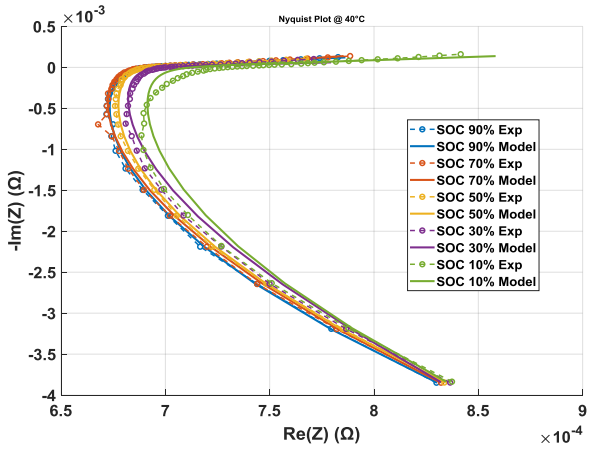

Figure 5: Nyquist plot of experimental and ECM model at 40°C and different SOC level

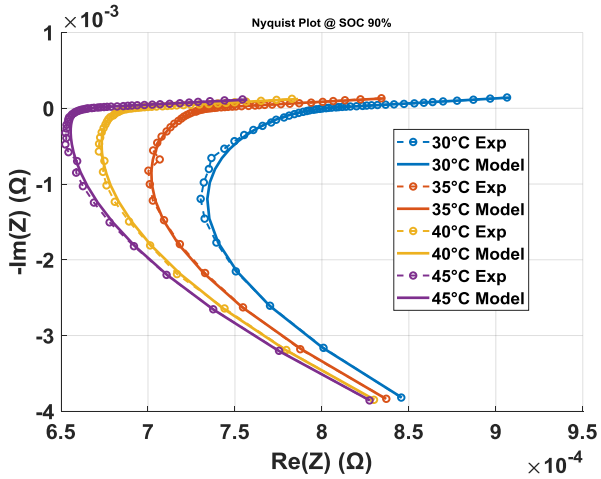

Figure 6: Nyquist plot of experimental and ECM model at 90% SOC and different temperature values

The variation of joule heat, the entropic heat, and the total heat generated as a function of SOC is demonstrated in Figure 7.

The result indicates that the joule heat dominates the heat generation at low SOC and decreases sharply as SOC increases, and this shows the battery has higher internal resistance at low SOC.

The entropic heat shows a transition from negative to positive with a peak value near mid SOC. This reflects the entropy change is associated with the electrochemical reactions, showing cooling at low SOC and heating from mid to high SOC.

The total heart generation, which sums both heat generations (joule and entropic heat), has a maximum at low SOC that is due to the resistive losses, and after around 10% SOC, relatively stable heat is shown with a small rise at mid SOC due to the entropic component.

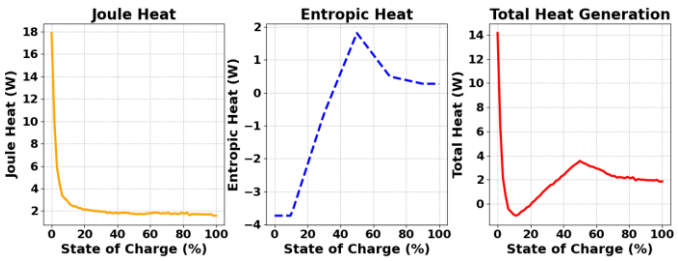

Figure 7: Heat generated Vs SOC

The total heat generated for the three charge/discharge cycles in Figure 8 shows a periodic spike in thermal output, particularly during discharging, which directly results in the temperature rise observed across the 15 sensor locations in Figure 9.

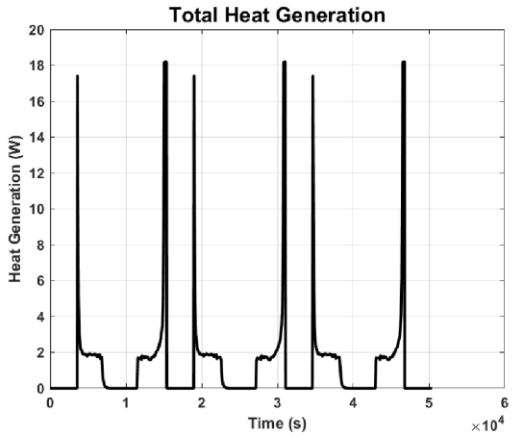

Figure 8: Heat generated Vs time

Figure 9 illustrates the comparison between the predicted and experimental surface temperatures of the 2D thermal model for all 15 thermocouple positions.

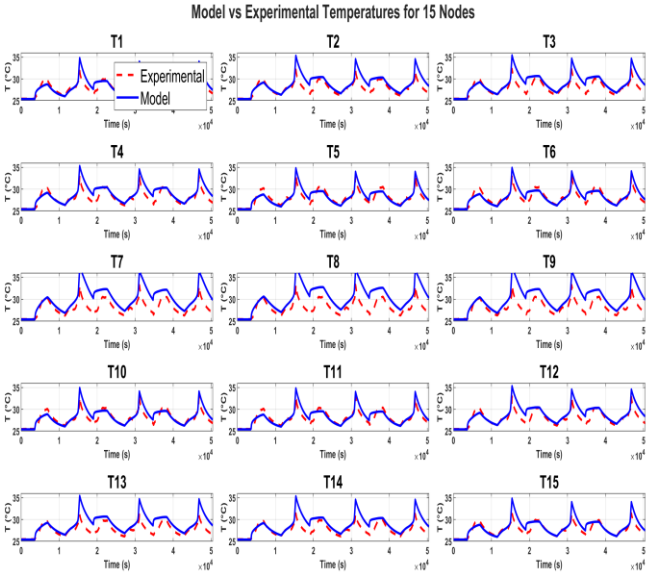

Figure 9: Experimental and predicted surface temperature

The result shows that the model prediction (solid blue line) yields a similar periodic pattern, indicating that the model captures the thermal dynamics across the cell surface. While the model captures well the experimental trends in most cases, minor deviations are noticed, especially at peak temperature values, suggesting further parameter refinement. In general, the 2D thermal model shows a good predictive capability, especially for distributed temperatures.

The capacity fade plot in Figure 10 indicates a close alignment between the model and experimental capacity fade. The experimental result shows a relatively stable capacity close to 100%, showing the battery is still in good health over the first 100 cycles. The capacity increase above 100% at the initial stage can be due to early electrochemical stabilization effects, such as continued SEI layer formation. The slight drop around cycle 35 is seen, which is due to a one-week rest period without cycling.

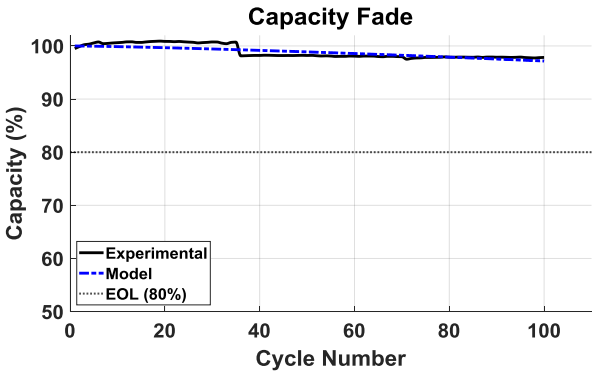

Figure 10: Experimental and predicted capacity fade

5 Conclusion and Perspective

This work established a multi-physical model for a high-capacity lithium-ion pouch cell that combines electrical, thermal, and aging dynamics into a single framework. By

coupling the ECM, 2D finite difference thermal model, and an Arrhenius law aging model, the model captures the key aspects of battery behaviour.

The experimental validation confirms that the integrated model can reproduce the electrical impedance of the battery across various SOC and temperature values, predict the spatial temperature distribution during cycling, and estimate the cell's capacity fade. These result shows the model's capability in predicting the thermal state, SOC, and SOH of the battery.

While the proposed model shows a strong agreement with experimental data, it is currently validated only for one cell chemistry (a 40 Ah NMC pouch cell) under limited cycling conditions. Future investigations will extend the model to other Li-ion chemistries, as they have different thermal properties and aging mechanisms.

Further refinement of the model's accuracy, including calibrating the aging model over a longer lifespan, is also planned. Scaling the model to the module level is another critical future investigation, as the module would allow the simulation of cell-to-cell thermal interactions.

6 REFERENCES

[1] J. Deng, C. Bae, A. Denlinger, et T. Miller, « Electric vehicles batteries: requirements and challenges », *Joule*, vol. 4, n° 3, p. 511‑ 515, 2020.

[2] A. García, J. Monsalve-Serrano, S. Martinez-Boggio, et D. Golke, « Energy assessment of the ageing phenomenon in Li-Ion batteries and its impact on the vehicle range efficiency », *Energy Convers. Manag.*, vol. 276, p. 116530, 2023.

[3] H. E. Perez, X. Hu, S. Dey, et S. J. Moura, « Optimal charging of Li-ion batteries with coupled electro-thermal-aging dynamics », *IEEE Trans. Veh. Technol.*, vol. 66, n° 9, p. 7761‑ 7770, 2017.

[4] H. Pasdarshahri, É. Veilleux, W. Mooney, L. G. Fréchette, F. Grondin, et D. Rancourt, « Coupled Electro-Thermal-Aging Battery Pack Modeling—Part 1: Cell Level », *Batteries*, vol. 10, n° 11, p. 404, 2024.

[5] H. Shi *et al.*, « Improved electric-thermal-aging multi-physics domain coupling modeling and identification decoupling of complex kinetic processes based on timescale quantification in lithium-ion batteries », *Appl. Energy*, vol. 353, p. 122174, 2024.

[6] S. Vaidya, D. Depernet, S. Laghrouche, et D. Chrenko, « State of temperature detection of Li-ion batteries by intelligent gray box model », *J. Power Sources*, vol. 585, p. 233624, 2023.

[7] X. Zhang, W. Zhang, et G. Lei, « A Review of Li-ion Battery Equivalent Circuit Models », *Trans. Electr. Electron. Mater.*, vol. 17, n° 6, p. 311‑ 316, déc. 2016, doi: 10.4313/TEEM.2016.17.6.311.

[8] B. Palmieri, F. Cilento, C. Siviello, F. Bertocchi, M. Giordano, et A. Martone, « Mitigation of heat propagation in a battery pack by interstitial graphite nanoplatelet layer: coupled electrochemical-heat transfer model », *J. Compos. Sci.*, vol. 6, n° 10, p. 296, 2022.

[9] C. Y. Guo, M. W. Muhieldeen, K. H. Teng, et A. Show, « A Critical Review of Advancements and Challenges in Thermal Management Systems For Lithium-Ion Batteries », *J. Adv. Res. Numer. Heat Transf.*, vol. 35, n° 1, p. 117‑ 161, avr. 2025, doi: 10.37934/arnht.35.1.117161.

[10] X. Cui *et al.*, « Optimization of the lumped parameter thermal model for hard-cased li-ion batteries », *J. Energy Storage*, vol. 32, p. 101758, 2020.

[11] C. Forgez, D. V. Do, G. Friedrich, M. Morcrette, et C. Delacourt, « Thermal modeling of a cylindrical LiFePO4/graphite lithium-ion battery », *J. Power Sources*, vol. 195, n° 9, p. 2961‑ 2968, 2010.

[12] J. Liu *et al.*, « Capacity fading mechanisms and state of health prediction of commercial lithium-ion battery in total lifespan », *J. Energy Storage*, vol. 46, p. 103910, 2022.

[13] S. S. Madani *et al.*, « A Comprehensive Review on Lithium-Ion Battery Lifetime Prediction and Aging Mechanism Analysis », *Batteries*, vol. 11, n° 4, p. 127, 2025.

7 ACKNOWLEDGMENT

This work has been supported by the EIPHI Graduate School (contract ANR-17-EURE-0002) and the Region Bourgogne Franche-Comté. Additionally, support was provided by the European Union through the Horizon Europe program and the innovation program under ‘‘GAP-101103667’’.